Materials Chemistry and Physics 240 (2020) 122246

Contents lists available at ScienceDirect

Materials Chemistry and Physics

journal homepage: www.elsevier.com/locate/matchemphys

Branched azomethines based on tris(2-aminoethyl)amine: Impact of imine core functionalization on thermal, electrochemical and luminescence properties

Danuta Sęk [a], Agata Szlapa-Kula [b], Mariola Siwy [a], Aleksandra Fabiańczyk [b], Henryk Janeczek [a], Marcin Szalkowski [c], Sebastian Maćkowski [c], Ewa Schab-Balcerzak [a,b,*]

[a] Centre of Polymer and Carbon Materials, Polish Academy of Sciences, 34 M. Curie-Sklodowska Str, 41-819, Zabrze, Poland
[b] Institute of Chemistry, University of Silesia, 9 Szkolna Str, 40-006, Katowice, Poland
[c] Institute of Physics, Faculty of Physics, Astronomy and Informatics, Nicolaus Copernicus University, Grudziadzka 5, 87-100, Torun, Poland

HIGHLIGHTS

- The impact of imine core functionalization was demonstrated.
- The derivatives were thermally stable with T_5 ranging from 140 to 294 °C.
- They were photoluminescent in solution and in the solid state.
- Their the energy band gap was between 2.10 and 2.38 eV being promising for organic electronics.
- The ability neat azomethines for electroluminescence was demonstrated.

GRAPHICAL ABSTRACT

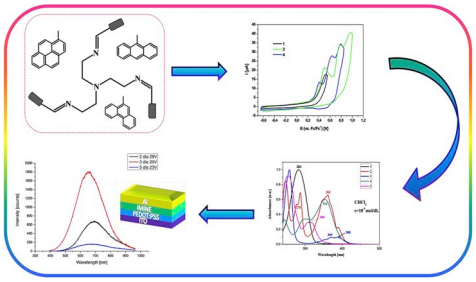

ARTICLE INFO

Keywords:
Tris(2-aminoethyl)amine derivatives
Imines
Luminescence
Electrochemistry

ABSTRACT

A series of imines based on tris(2-aminoethyl)amine was designed and synthesized to evaluate the effect of core functionalization with biphenyl, pyrene, anthracene, triphenylamine and phenanthrene units on selected properties. Their chemical structure was thoroughly characterized by NMR and FTIR spectroscopy and elemental analysis. All compounds were crystalline (except for imine with triphenylamine units) and melted in the wide temperature range of 99–187 °C, according to the structure of the substituent. DSC measurements revealed that the studied compounds can be converted into amorphous material with glass transition occurring for temperatures between 16 and 55 °C. The imines were electrochemically active and underwent oxidation and reduction processes as found using CV and DPV methods. Density functional theory was employed for optimizing the imines geometry, as well as for calculating HOMO and LUMO orbital energies together with ionization potentials and electron affinities. The absorption and photoluminescence in the UV–Vis spectral range, both in solution and in the solid state as films on glass substrates were studied. When dissolved in chloroform, they emitted light with quantum yields ranging from 0.54 to 22%. In the solid state they exhibited emission in the range of 380–515 nm. The selected compounds were preliminarily tested as components in light emitting diodes. The ability neat azomethines for electroluminescence in diode ITO/PEDOT:PSS/imine/Al was demonstrated.

* Corresponding author. Centre of Polymer and Carbon Materials, Polish Academy of Sciences, 34 M. Curie-Sklodowska Str, 41-819, Zabrze, Poland.
E-mail address: ewa.schab-balcerzak@us.edu.pl (E. Schab-Balcerzak).

https://doi.org/10.1016/j.matchemphys.2019.122246
Received 9 May 2019; Received in revised form 5 August 2019; Accepted 30 September 2019
Available online 1 October 2019

1. Introduction

In the last decades, imine compounds (also known as azomethine or Schiff bases) have gained popularity due to the possibility of their use in many aspects of science, such as: organic synthesis, analytical and coordination chemistry, biology, medicine, and pharmacy, as well as in photovoltaics and optoelectronics [1–13]. In most cases, amines used for the azomethines synthesis possess aromatic or heteroaromatic structures. There are also reports describing imines prepared using aliphatic amines, such as tris-(2-aminoethyl)amine. Azomethines prepared from tris-(2-aminoethyl)amine have been discussed in terms of their anticancer [14–17], and anti-inflammatory [18] properties. There are also some examples of using these compounds as colorimetric and fluorescence chemosensors [19,20] and liquid crystalline materials [21].

In this paper a series of imines obtained by condensation of tris-(2-aminoethyl)amine with the following aldehydes: biphenyl-4-carboxaldehyde, 4-(diphenylamino)benzaldehyde, 9-anthracenecarboxaldehyde, 1-pyrenecarboxaldehyde, and 9-phenanthrenecarboxaldehyde are presented. Two of them have been described in the literature, but their optoelectronic properties have not been reported [22,23]. Ravikumaret et al. [22] synthesized tris-[2-(9′-anthracene) iminoethyl]amine and used it as a substrate in reduction reaction to receiving a hydrogenated form of Schiff base. Afterward, the compound and its derivative with p-nitrobenzyl and p-methoxybenzyl moieties were tested for application as fluorophores for metals' detection. Wenzel et al. [23] described tris[2-(4′-phenylbenzyl)iminoethyl]amine as a ligand for studying the properties of its complexes with silver. Our study concerns azomethines with tris(2-aminoethyl)amine as a core being further functionalized with biphenyl, pyrene, anthracene, triphenylamine, and phenanthrene units. These compounds were investigated mainly from the point of view of their thermal and optical properties. Moreover, preliminary tests of using these molecules as materials in optoelectronic devices were also carried out.

2. Experimental section

2.1. Materials

Tris-(2-aminoethyl)amine (96%) (Tris), biphenyl-4-carboxaldehyde (99%), 4-(diphenylamino)benzaldehyde (97%), 9-anthracenecarboxaldehyde (97%), 1-pyrenecarboxaldehyde (99%), and 9-phenanthrenecarboxaldehyde (97%) were purchased in Aldrich and used as received. Methanol, ethanol, chloroform, isopropyl alcohol, and NaOH were obtained from POCH. Poly(3,4(ethylenedioxy)thiophene): polystyrene sulfonate (PEDOT:PSS) and ITO glass were purchased from OSSILA.

2.2. Synthesis of imines

0.5 mmol of tris-(2-aminoethyl)amine and 1.5 mmol of biphenyl-4-carboxaldehyde and other aldehydes (1-pyrenecarboxaldehyde, 9-anthracenecarboxaldehyde, 4-(diphenylamino)benzaldehyde or 9-phenanthrenecarboxaldehyde) were dissolved in 6 ml of chloroform (imine 1) or ethanol (other imines). The solutions were heated to 50 °C under argon atmosphere for one week (imine 1) or two weeks (other imines). The solvent was evaporated and the product was washed several times with methanol and dried at 60 °C in vacuum.

2.2.1. Tris[2-(4′-phenylbenzyl)iminoethyl]amine (1)

The product was received as yellow solid. Yield: 30%; ^{1}H NMR ($CDCl_3$, δ, ppm): 8.16 (s, -CH=N, 3H), 7.61–7.57 (m, 12H_{Ar}), 7.56–7.54 (m, 6H_{Ar}), 7.45–7.42 (m, 6H_{Ar}), 7.37 (m, 3H_{Ar}), 3.74 (m, 6H_{Al}), 2.98 (t, $J = 6.3$ Hz, 6H_{Al}). ^{13}C NMR ($CDCl_3$, δ, ppm): 161.68 (-CH=N), 143.23, 140.50, 135.35, 128.98, 128.65, 127.82, 127.33, 127.21, 60.28, 55.79. FTIR (cm^{-1}): 3054, 3030 (C–H aromatic), 2826, 2923 (-CH_2-), 1642 (CH=N), 1580 (C=C) stretching deformation in phenyl ring), 1227 (C–N stretching); Elem. anal. for $C_{45}H_{42}N_4$ (638.84 g/mol): found (calcd) % C 84.39 (84.60), H 6.57 (6.63), N 8.64 (8.77).

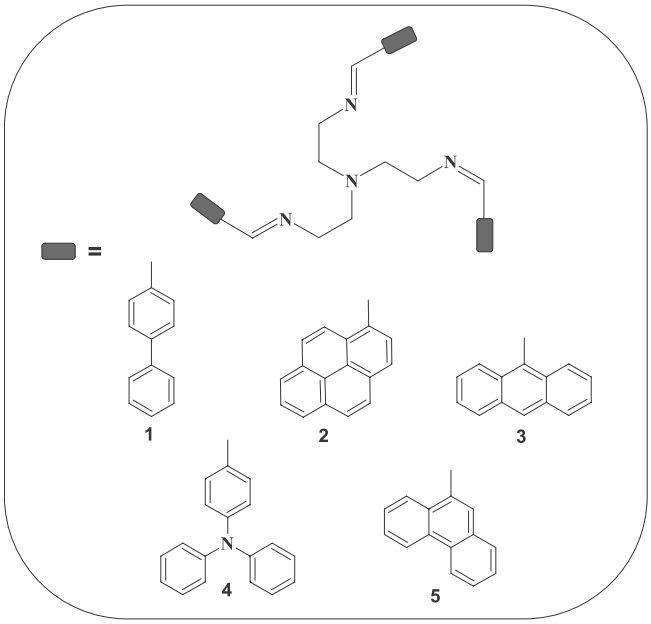

Fig. 1. The chemical structure of the synthesized imines.

Table 1
^{1}H NMR and ^{13}C NMR signals of the protons in N(-$C^{\beta}H_2$-$C^{\alpha}H_2$-N=CH-Ar)$_3$.

Code	^{1}H NMR/^{13}C NMR signals in the imines [ppm]			Down-field shift[a] after condensation [ppm]	
	-N=CH-	-$C^{\alpha}H_2$-	-$C^{\beta}H_2$-	-$C^{\alpha}H_2$-	-$C^{\beta}H_2$-
1	8.16/161.68	2.98/60.28	3.74/55.79	0.59	1.11
2	9.09/160.78	3.26/61.44	4.04/56.18	0.87	1.41
3	9.38/161.46	3.41/61.43	4.23/55.84	1.02	1.60
4	8.01/161.41	2.90/60.16	3.65/56.08	0.51	1.02
5	8.71/162.53	3.21/61.47	3.94/56.30	0.82	1.31

[a] Aliphatic hydrogens down-field shift signals after condensation in comparison with the proper signals in tris (2-aminoethyl)amine Hα = 2.39 ppm, Hß = 2.63 ppm.

2.2.2. Tris[2-(1′-pyrene)iminoethyl]amine (2)

The product was received as white solid. Yield: 25%; ^{1}H NMR ($CDCl_3$, δ, ppm) δ 9.09 (s, -CH=N, 3H), 8.45 (d, $J = 9.3$ Hz, 3H_{Ar}), 8.27 (d, $J = 8.0$ Hz, 3H_{Ar}), 8.04 (dd, $J = 6.9$, 1.7 Hz, 3H_{Ar}), 7.91–7.87 (m, 6H_{Ar}), 7.86 (d, $J = 8.8$ Hz, 3H_{Ar}), 7.82 (d, $J = 8.0$ Hz, 3H_{Ar}), 7.73 (d, $J = 8.8$ Hz, 3H_{Ar}), 7.62 (d, $J = 9.3$ Hz, 3H_{Ar}), 4.06–4.02 (m, $J = 6.2$, 5.3 Hz, 6H_{Al}), 3.26 (t, $J = 6.1$ Hz, 6H_{Al}). ^{13}C NMR ($CDCl_3$, δ, ppm): 160.78 (-CH=N), 132.51, 131.12, 130.43, 129.54, 128.62, 128.24, 127.22, 125.99, 125.89, 125.64, 125.41, 124.79, 124.54, 124.41, 122.32, 117.05, 61.44, 56.18. FTIR (cm^{-1}): 3039 (C–H aromatic), 2923, 2837, 2805 (-CH_2-), 1634 (-CH=N stretching), 1595 (C=C stretching deformation in phenyl ring), 1245 (C–N stretching). Elem. anal. for $C_{57}H_{42}N_4$ (782.97 g/mol): found (calcd) % C 86.96 (87.44), H 5.50 (5.41), N 7.05 (7.15).

2.2.3. Tris[2-(9′-antracene)iminoethyl]amine (3)

The product was received as orange solid. Yield: 31%; ^{1}H NMR ($CDCl_3$, δ, ppm) δ 9.38 (s, -CH=N, 3H), 8.49–8.46 (m, 6H_{Ar}), 8.33 (s, 3H_{Ar}), 7.92–7.90 (m, 6H_{Ar}), 7.41–7.38 (m, 12H_{Ar}), 4.24–4.21 (m, 6H_{Al}), 3.41 (t, $J = 6.7$ Hz, 6H_{Al}). ^{13}C NMR ($CDCl_3$, δ, ppm): 161.46 (-CH=N), 131.26, 129.99, 129.26, 128.86, 128.11, 126.63, 125.20, 124.96, 61.43, 55.84. FTIR (cm^{-1}): 3047 (C–H aromatic), 2923, 2826 (-CH_2-), 1636 (-CH=N stretching), 1519 (C=C stretching deformation in phenyl ring), 1254 (C–N stretching). Elem. anal. for $C_{51}H_{42}N_4$ (710.90 g/mol): found

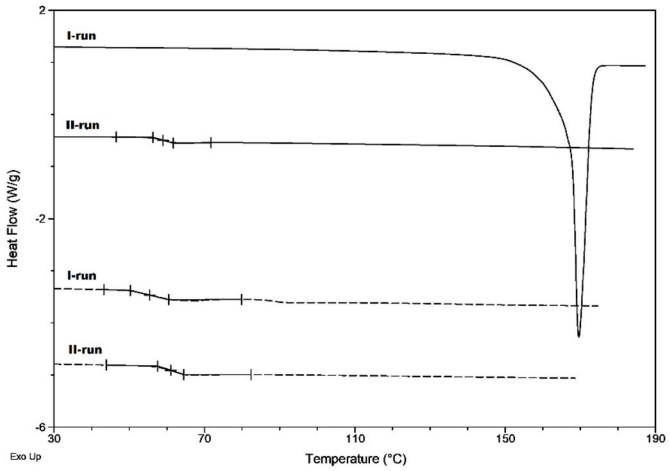

(b)

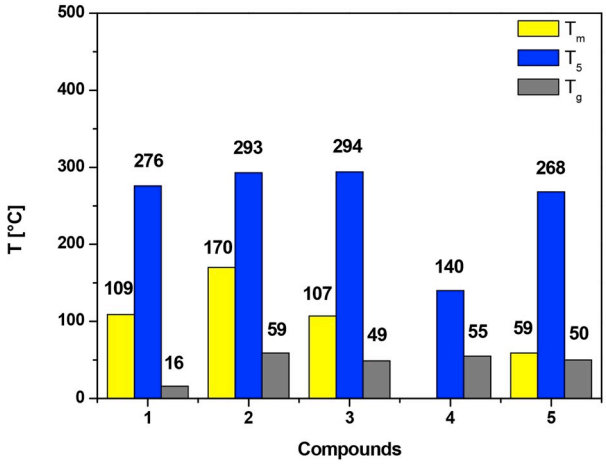

Fig. 2. (a) DSC curves of **2** (straight line) and **4**(dotted line) registered at a first and second heating run (scan rate 10 °C/min) and (b) melting (T_m), glass transition (T_g) and 5% weight loss (T_5) temperatures of imines.

(calcd) % C 86.16 (86.16), H 6.07 (5.96), N 7.84 (7.88).

2.2.4. *Tris[2-(4′-diphenyloamino)iminoethyl]amine (4)*

The product was received as orange crystals. Yield: 28%; ^{1}H NMR ($CDCl_3$, δ, ppm): 8.01 (s, -CH=N, 3H), 7.38–7.36 (m, 6H_{Ar}), 7.23–7.21 (m, 12H_{Ar}), 7.08–7.06 (m, 12H_{Ar}), 7.05–7.03 (m, 6H_{Ar}), 7.00–6.98 (m, 6H_{Ar}), 3.65 (t, $J = 6.0$ Hz, 6H_{Al}), 2.90 (t, $J = 6.2$ Hz, 6H_{Al}). ^{13}C NMR ($CDCl_3$, δ, ppm): 161.41 (-CH=N), 147.29, 146.31, 129.87, 129.54, 126.46, 125.31, 125.25, 119.50, 60.16, 56.08. FTIR (cm^{-1}): 3058, 3032 (C–H aromatic), 2832, 2923 (-CH_2-), 1641 (-CH=N stretching), 1589 (C=C stretching deformation in phenyl ring), 1280 (C–N stretching). Elem. anal. for $C_{63}H_{57}N_7$ (912.17 g/mol): found (calcd) % C 81.86 (82.95), H 6.40 (6.3), N 10.55 (10.75).

2.2.5. *Tris[2-(9′-phenanthrene)iminoethyl]amine (5)*

The product was received as yellow solid. Yield: 25%; ^{1}H NMR ($CDCl_3$, δ, ppm): 9.04 (dd, $J = 8.3$, 1.0 Hz, 3H_{Ar}), 8.71 (s, -CH=N, 3H), 8.61–8.59 (m, 3H_{Ar}), 8.55 (d, $J = 8.2$ Hz, 3H_{Ar}), 7.63–7.60 (m, 6H_{Ar}), 7.58 (m, 3H_{Ar}), 7.53–7.48 (m, 6H_{Ar}), 7.44 (m, 3H_{Ar}), 3.96–3.92 (m, 6H_{Al}), 3.21 (t, $J = 6.2$ Hz, 6H_{Al}). ^{13}C NMR ($CDCl_3$, δ, ppm): 162.53 (-CH=N), 131.40, 131.20, 130.98, 130.68, 130.30, 129.82, 129.51, 127.84, 127.16, 126.77, 126.72, 125.71, 122.92, 122.53, 61.47, 56.30. FTIR (cm^{-1}): 3077, 3054 (C–H aromatic), 2923, 2832 (-CH_2-), 1640 (-CH=N stretching), 1527 (C=C stretching deformation in phenyl ring), 1247 (C–N stretching). Elem. anal. for $C_{51}H_{42}N_4$ (710.90 g/mol): found (calcd) % C 85.96 (86.16), H 5.65 (5.95), N 7.30 (7.88).

3. Results and discussion

3.1. *Synthesis and structural characterization*

Five imines being the condensation products of tris(2-aminoethyl) amine with different aldehydes were synthesized and investigated. The imines were designed to evaluate the effect of core functionalization with biphenyl, pyrene, anthracene, triphenylamine and phenanthrene units on selected thermal, redox and optical properties. The chemical structure of the prepared imines is depicted in Fig. 1.

Structures of the compounds were confirmed by instrumental techniques including ^{1}H NMR, ^{13}C NMR, FTIR, and elemental analysis. The selected NMR data are collected in Table 1, whereas all signals are listed in the Experimental section and the representative ^{1}H NMR and ^{13}C NMR spectra are given in Fig.1S and 2S.

Signals of protons in imine groups were found in the range of 8.01–9.38 ppm. It should be stressed that in the compounds bearing condensed aromatic rings i.e. with pyrene (**2**), anthracene (**3**) and phenanthrene (**5**) units, the higher downfield shift of the imine protons was observed in comparison with the ones with phenyl unit, i.e. biphenyl (**1**) and triphenylamine (**4**). Two signals of triamine aliphatic protons were also down-field shifted after condensation amine groups with an aldehyde. However, the downfield shift of the proton signals being bond to carbon atom closer to imine groups was smaller than the signals of the protons at carbon atom closer to the nitrogen atom in the center of the triamine. If one takes into consideration the structure of

Table 2
Redox potentials, ionization potentials (IP), electron affinities (EA) and energy band gap (E_g) of investigated imines.

Code	E_{1red} [V]	E_{2red} [V]	E_{1ox} [V]	E_{2ox} [V]	E_{3ox} [V]	IP[a] (CV)	EA[b] (CV)	IP (DFT)	EA (DFT)	$E_{g(CV)}$[c] [eV]	$E_{g(DFT)}$ [c] [eV]	$E_{g(OPT)}$[d] [eV]
1	−2.11 (−2.13)	−2.39 (−2.37)	0.27 (0.22)	0.83 (0.75)	–	−5.37	−2.99	5.51	2.06	2.38	3.46	3.82
2	−1.87 (−1.93)	−2.15 (−2.19)	0.24 (0.15)	0.64 (0.54)	–	−5.34	−3.23	5.45	2.46	2.11	2.99	3.02
3	−1.71 (−1.72)	−2.02 (−2.03)	0.39 (0.31)	0.65 (0.63)	0.86 (0.80)	−5.49	−3.39	5.55	2.55	2.10	3.01	2.92
4	−2.26 (−2.29)	–	0.31 (0.27)	0.48 (0.40)	0.7 (0.64)	−5.41	−2.84	5.29	1.84	2.57	3.46	3.08
5	−2.01 (−2.06)	−2.26 (−2.28)	0.35 (0.28)	1.39 (1.39)	–	−5.45	−3.09	6.05	2.16	2.36	3.88	3.59

[a] IP = −5.1 - E_{ox}.
[b] EA = −5.1 – E_{red}.
[c] $Eg_{(CV)} = E_{ox\ (onset)} - E_{red\ (onset)}$.
[d] $E_{g(OPT)} = 1240/\lambda_{onset}$ [26].

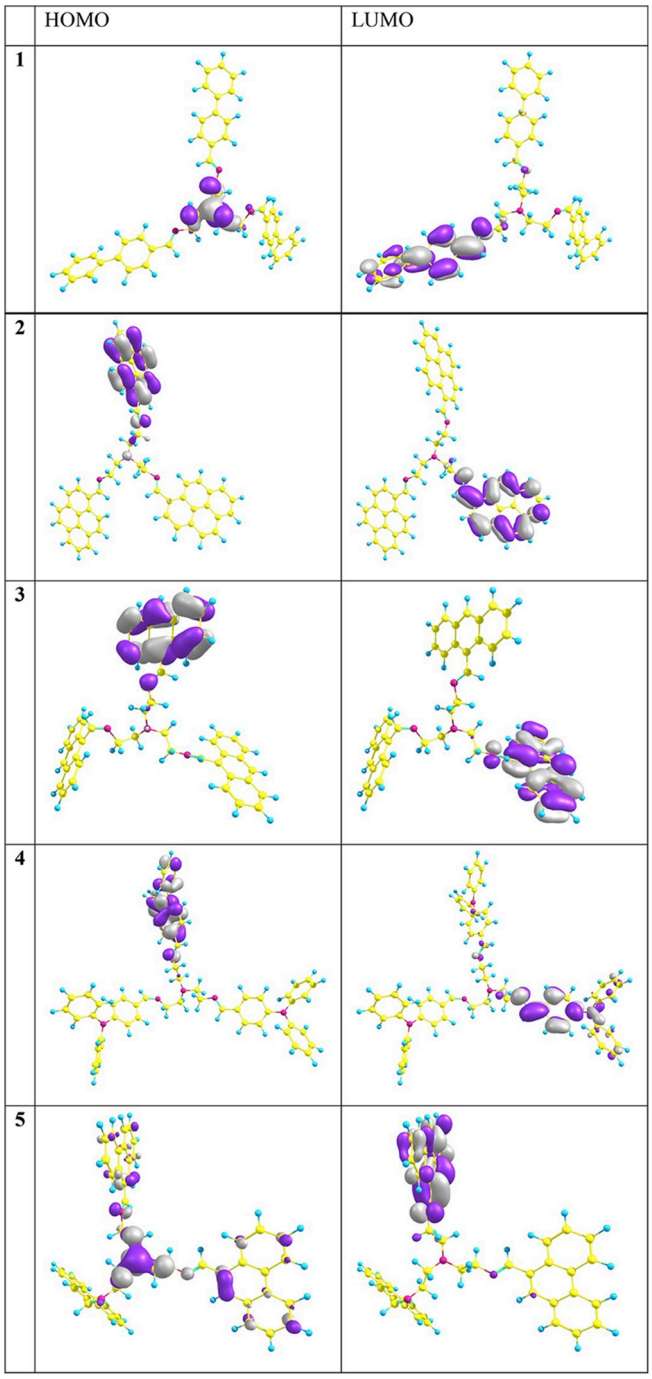

Fig. 3. HOMO, LUMO energies and contours of the synthesized imines.

aldehyde, it can be seen that pyrene, anthracene and phenanthrene moieties caused bigger downfield shifts of the aliphatic protons than the biphenyl and triphenylamine units in the compounds.

Signals of azomethine carbon atoms in ^{13}C NMR were found in the range of 160.78–162.53 ppm. The signal at the low field was detected for the compound with phenanthrene units (**5**) and at the highest field for the compound with pyrene moieties (**2**). Signals of the aliphatic carbons being bond to the imine group (α in Table 1) were detected in the range of 60.16–61.47 ppm, while the carbon atoms connected with nitrogen the center of triamine were found in the range of 55.79–56.30 ppm.

In FTIR spectra (cf. Fig. 4S) absorption bands of imine groups were detected in the range of 1642-1634 cm^{-1} and the little higher frequency was observed in the compounds with biphenyl (**1**), triphenylamine (**4**) and phenanthrene (**5**) moieties. Absorption bands typical for aromatic and aliphatic structures were also present in the FTIR spectra of the compounds (cf. Experimental part and Fig. 4S).

3.2. TGA and DSC studies

Thermogravimetric analysis (TGA) and differential scanning calorimetry (DSC) was applied to estimate the thermal behavior of the prepared imines. Fig. 2 presents representative DSC thermograms and thermal data of this family of compounds. The DSC and TGA thermograms of the other imines are depicted in Fig. 3S.

The TGA analysis indicates that the initial thermal decomposition of the imines - based on a temperature of 5% weight loss (T_5) - was in the range of 140–294 °C. It was found that the substitution of the imine core with triphenylamine units (**4**) significantly lowered thermal stability compared to the others substituents.

All the azomethines except for the molecule with triphenylamine units (**4**) were obtained after synthesis as crystalline solids and at the first heating scan gave similar DSC profiles with melting endotherms. In the case of the mentioned imine **4** during the first heating run only glass transition temperature (T_g) was detected. After rapid cooling, during the second heating, only T_g was seen. That means that the compounds did not form a crystalline structure after rapid cooling. The imines with anthracene (**3**) and pyrene (**2**) structures exhibited the highest melting points (cf. Fig. 2b). A minor effect of triamine substituent structure on T_g was found except for **1**. The presence of biphenyl units significantly lowered the T_g from about 50 to 16 °C.

3.3. DFT geometry optimization

Theoretical calculations allow enriching the experimental results. The knowledge gained from the DFT calculations allows for a better understanding of the molecules studied. Therefore, the presented compounds were calculated using Gaussian16 program [24]. The calculations were used the hybrid B3LYP function along with the 6–31++G** (d,p) basis set. All theoretical results carried out in dichloromethane and the data obtained are collected in Table 2 and Fig. 3.

As can be seen, the compounds are characterized by complicated structures. Nevertheless, the LUMO orbitals are located on one of three substituents in each molecule. They also include binding –C=N-. In the case of HOMO orbitals, the situation is different. For compounds **1** and **5** these orbitals concentrate generally on the central nitrogen. On the other hand, in **2**, **3** and **4** HOMOs are localized in pyrene, anthracene, and triphenylamine group, respectively. For all the imines, IP and EA and E_g were calculated. Comparing the values obtained for individual compounds, we can conclude that the greatest impact on the received data is related to the triphenylamine units. The rest of the aryl compounds are similar in values (in terms of IP). If we take into account E_g values, the most promising compound is **2,** because the energy gap is the smallest, which makes it easier to transfer electrons.

3.4. Electrochemical behavior

Electrochemical measurements allow a preliminary assessment of the behavior of compounds under the influence of the applied voltage. The determination of parameters, such as electron affinity (EA) or ionization potential (IP) allows the selection of appropriate materials for layers in electronic devices. Therefore, the electrochemical behavior of presented imines was tested using cyclic voltammetry (CV) and differential pulse voltammetry (DPV) in dichloromethane. Onsets of electrochemical oxidation and reduction potentials were used to designate IP and EA (assuming that IP of ferrocene equals −5.1 eV) [25]. Representative voltammograms are presented in Fig. 4, whereas the CV and DPV data are collected in Table 2.

All of the investigated branched azomethines were electroactive and

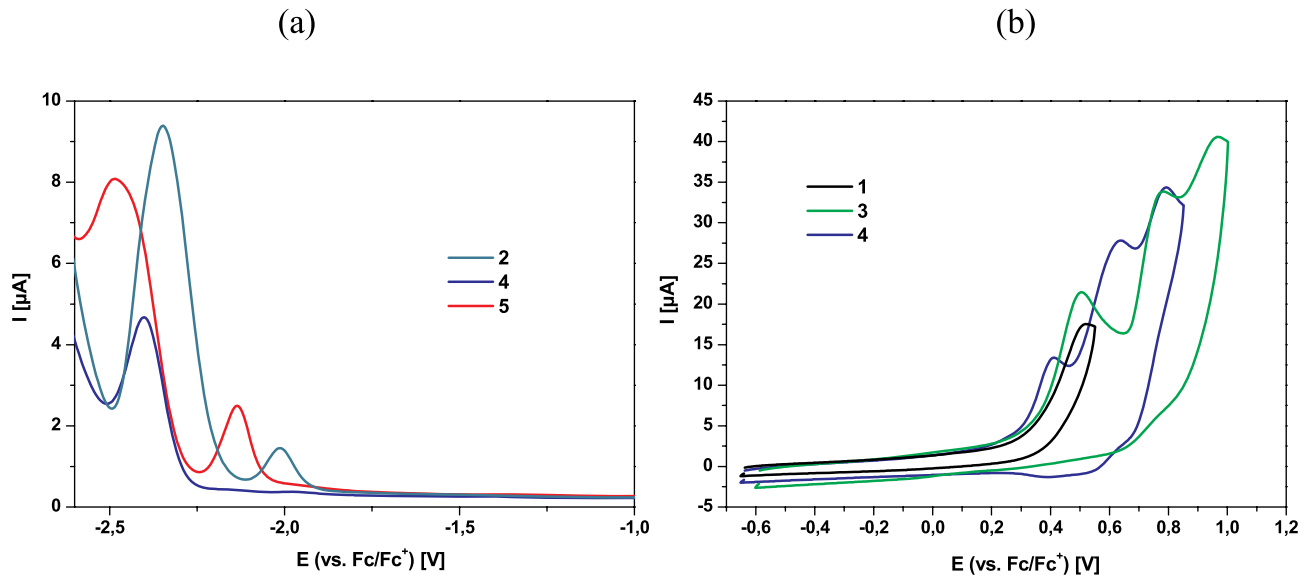

Fig. 4. (a) DPV spectra of reduction processes for 2, 4 and 5 compounds (b) CV spectra of oxidation processes for 1, 3 and 4. All spectra were registered in dichloromethane with 0.1 M Bu_4NPF_6.

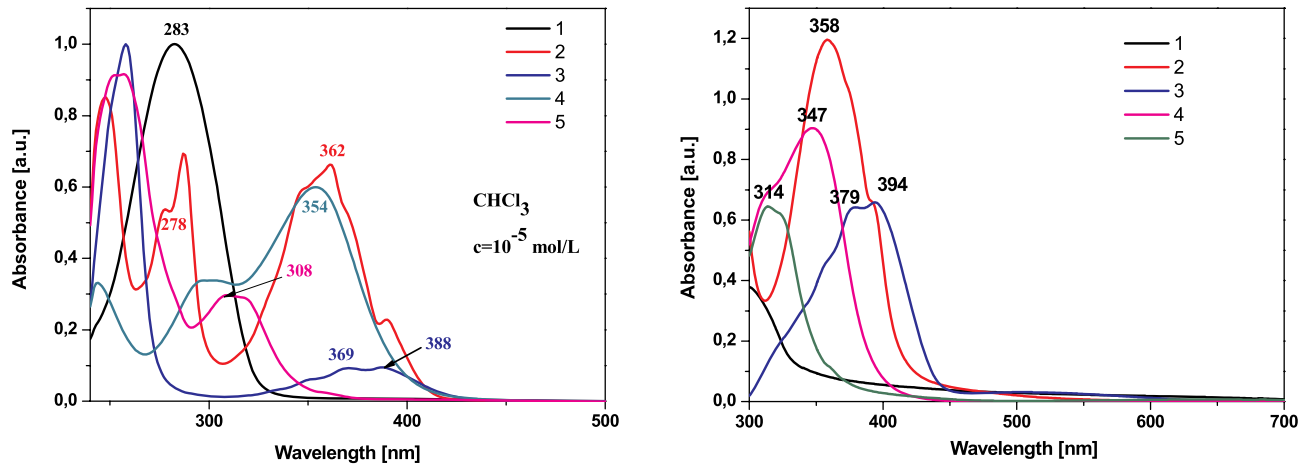

Fig. 5. Absorption spectra of azomethines in (a) chloroform and (b) as a film.

Table 3
UV–Vis and PL spectroscopic data of azomethines.

Code	Absorption λ_{max} [nm] (ε x10^4 [$dm^3 \cdot mol^{-1} cm^{-1}$])		Photoluminescence λ_{em}[nm] (Φ_{PL} [%])		Stokes shift[c] $\Delta\nu$ [cm^{-1}]	
	Solution[a]	Film	Solution[b]	Film	Solution	Film
1	283 (10.0)	300	407 (2.8)	454	10766	11499
2	248 (8.5), 278 (5.4), 287 (6.9), 362 (6.6), 390 (2.3)	358	422, 505 (21.0)	515	7822	8515
3	258 (10.0), 369 (0.9), 388(0.9)	379, 394	441 (0.5), 466[sh]	438	3097	2550
4	244 (3.3), 296 (3.4), 354(6.0)	347	438 (22.0)	445 (2.5)	5418	6792
5	257 (9.2), 308 (3.0)	314	376 (0.7), 498	380 (0.5)	5872	5531

[a] $c = 10^{-5}$mol/dL.
[b] $c = 10^{-4}$mol/dL.
[c] $\Delta\nu = (1/\lambda_{abs} - 1/\lambda_{em}) \cdot 10^7$ [cm^{-1}].

undergo oxidation and reduction processes. In the negative potential range (vs Fc/Fc+) one or two cathodic peaks in the range from −1.71 to −2.39V were distinguished. Imine containing triphenylamine substituents (**4**) differed from other derivatives (cf. Fig. 4a). The reduction process, in this case, was one-stage and amounted to −2.26 V. Presented values of the discussed process for all azomethines indicate that the reduction may occur on the -C=N- moiety. In addition, the introduction of aromatic units into the molecule, e.g. anthracene or phenanthrene, reduces the value of the reduction potential, which confirms literature reports [8,27]. Subsequently, in the positive potential range, the imines were tested. All compounds exhibited a multistage oxidation process with anodic peaks in the range of 0.24–1.39 V. It is interesting to note that for all derivatives the E_{1ox} values are very similar (what can be seen Fig. 4b). Such low oxidation values for azomethines with aryl groups have been reported also in the literature [28]. Small differences in oxidation peak affect the significant similarity of IP values in the tested compounds, despite a large substituent diversity. In the case of EA, a larger distribution of values was seen. Comparing the values of E_g, it was seen that the presence of pyrene (**2**) and anthracene (**3**) substituents lowered energy band gap to ca. 2.1 eV.

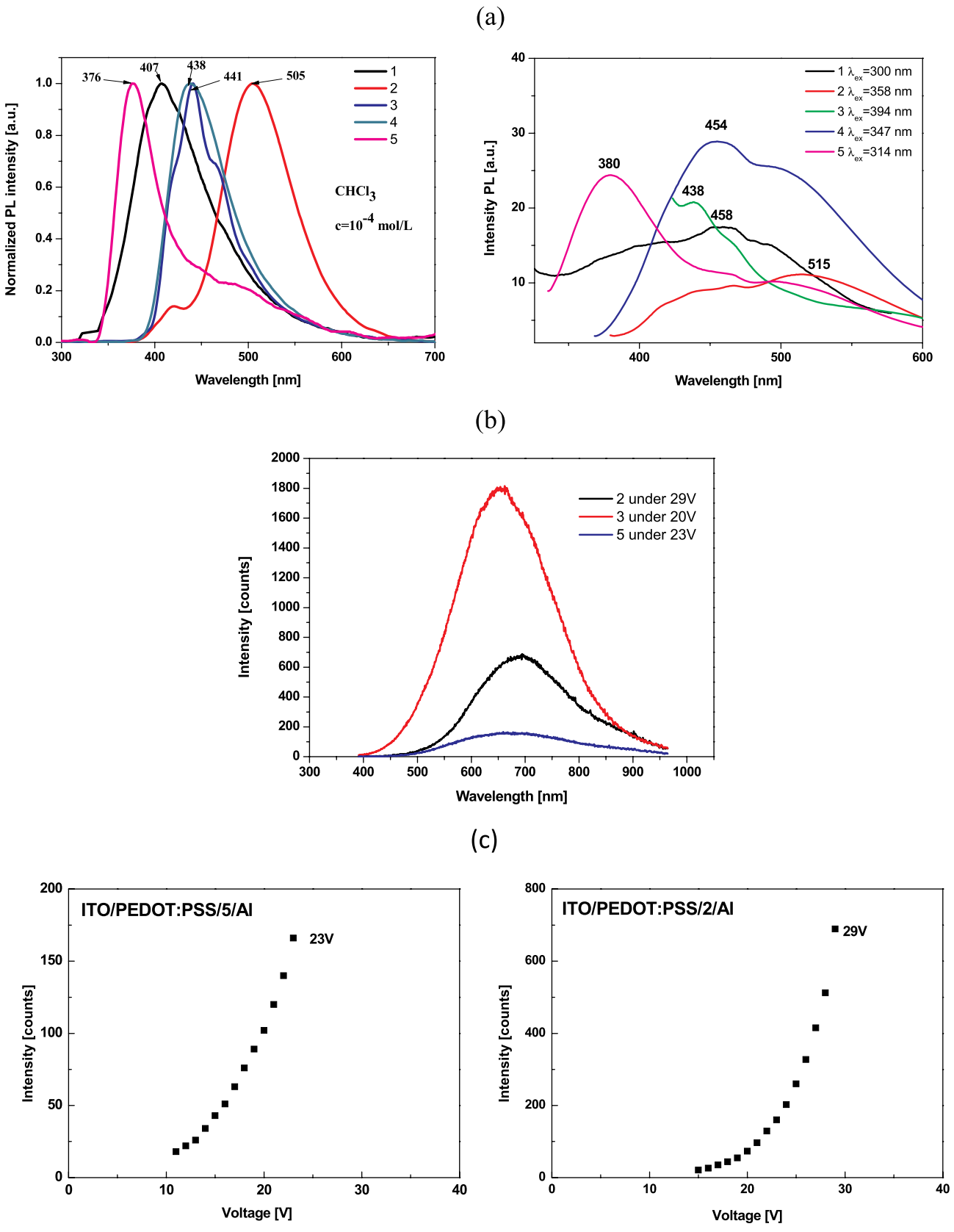

Fig. 6. (a) Photoluminescence spectra of the azomethines in solution (left side) and in the film (right side), (b) electroluminescence spectra of diodes based on **2**, **3** and **5** and (c) intensity of emitted light depending on voltage for device containing imine **2** and **5**.

3.5. Absorption and emission spectroscopy

The optical properties of the imines were studied by absorption and fluorescence emission spectroscopy. UV–Vis absorption and emission properties were investigated in chloroform solution and in the solid state as a thin film. Experimental UV–Vis spectra are presented in Fig. 5 and the spectroscopic data are collected in Table .3. For selected compounds (**1** and **5**) the TD-DFT calculations were performed. The results were added to the SI (Fig 5S and 6S).

UV–Vis spectra of the azomethines in solution consist of one (**1**), two (**3, 5**) or three (**2, 4**) bands with maximum (λ_{max}) located below 300 nm and in the range between 309 and 388 nm. As we can see, the simulated UV–Vis spectra showed good agreement with experimental data. For compound **1**, calculated transitions in the range from 317 to 279 nm can be observed. In the first and second absorption bands, we have the main contribution to the HOMO/LUMO +2 (84%) and HOMO/LUMO+1 (96%) orbitals. Other of them are more composited with smaller contributions. In the case of the compound **5**, we can distinguish three calculated main absorption bands HOMO/L+1 (43%), H-3/LUMO (58%) and H-2/L+2 (41%) corresponding to first band maximum (λ_{max}) located at 309 nm. For $\lambda_{max} = 257$ nm absorption band H-6/L+3 has the largest contribution of 75%. It was found that imines with pyrene (**2**), anthracene (**3**) and triphenylamine (**4**) groups absorbed the radiation from the lower energy region as compared to the others.

Electronic absorption spectra were also registered for thin films prepared from the imines. UV–Vis spectra of the films are showed in Fig. 5b.The films were cast from the compounds dissolved in $CHCl_3$. The absorption bands in films were slightly bathochromically shifted in comparison with the ones detected in $CHCl_3$ solution, except for the compound bearing triphenylamine moieties (cf. Table 3). In the case of the film of the compound with anthracene units, its absorption band consists of two overlapped bands, similar as it was detected for this compound in solution.

All imines were fluorescent in $CHCl_3$ solution and the position of maximum emission band (λ_{em}) was found in between 407 and 422 nm with one exception of the imine with phenanthrene units (**5**), which emitted light in the UV–Vis range. Photoluminescence spectra of the compounds in the film are presented in Fig. 6 and the maxima of emission band are collected in Table .3. Emission wavelengths of the compounds bearing anthracene (**3**) and triphenylamine (**4**) units are little different in solution. The imine with phenanthrene moieties (**5**) emits radiation with λ_{em} located at ca. 380 nm being hypsochromically shifted compare to the others. On the other hand, the compound with pyrene substituents (**2**) in $CHCl_3$ emitted light with λ_{em} bathochromically shifted to 505 nm. In most cases, the emission bands in the films are bathochromically shifted in comparison with that detected in solution except for the imine with anthracene units.

Photoluminescence efficiency is very important for practical application of the material, thus PL quantum yields (Φ_{PL}) of all azomethines in solution was measured. The highest PL quantum yield was found for the imines bearing pyrene (**2**) and triphenylamine (**4**) units. The presence of biphenyl (**1**) and surprisingly anthracene (**3**) and phenanthrene (**4**) derivatives significantly decrease the Φ_{PL} below 3 and 1%, respectively. The PL ability of imines in the form of the thin film was also examined because of the real applications require solid state samples. The imines were emissive, however, its photoluminescence intensity was lower compared to solution due to frequently observed PL quenching effect in solid state [29]. Photoluminescence Φ_{PL} of films was measured for two selected compounds, i.e. bearing triphenylamine (**4**) and phenanthrene (**5**) units and was found to be 2.5 and 0.5%, respectively.

Preliminary testing of electroluminescence (EL) ability of the synthesized imines in diodes with a configuration of ITO/PEDOT:PSS/imine/Al was carried out. The investigations were based on registering EL spectra under different values of the applied voltage. At this preliminary stage of work the typical diode parameters were not measured. Diode based on imine with biphenyl units (**1**) was non-emissive and surprisingly, the diode containing as an emissive layer the imine with triphenylamine structure (**4**) exhibited practically negligible emission of light. The other devices emitted light with a maximum of emission band λ_{EL} located at 545, 560 and 570 nm for a diode with azomethine **2**, **3** and **5**, respectively (cf. Fig. 6b). Together with the increase of the value of the external voltage the gradually higher luminescence intensity was observed (cf. Fig. 6b). The more intense light emission exhibited device based on imine with anthracene units (3). Considering the work function of cathode 4.3 eV [30,31] and EA of the investigated imines (cf. Table 2), which is closely related to LUMO energy level, the compound **3** exhibited the lowest value. The appropriate matching of HOMO and LUMO energy of compounds used for diode construction is crucial for efficient excitons recombination resulted in efficient diode performance [32]. Appropriate LUMO energy may facilitate the electron transfer from Al to the emissive layer.

4. Conclusions

Five branched azomethines with tris(2-aminoethyl)amine core were synthesized to investigate the impact of core functionalization on thermal, redox, UV–vis absorption, and luminescence properties. Considering the obtained results it can be pointed out:

- the presence of anthracene and pyrene units significantly raising T_m to compare to phenanthrene and biphenyl structure,
- imine with triphenylamine moieties was obtained as an amorphous compound, while the others can be converted into amorphous material, however with low T_g not exceed 60 °C,
- the replacement of triphenylamine units by others reduced the E_g value. The lowest E_g (2.1 eV) showed imines with anthracene and pyrene moieties,
- the highest PL quantum yield exhibited azomethines bearing triphenylamine and pyrene substituents,
- imines with pyrene, anthracene and phenanthrene units emitted green light under external voltage and the highest intensity of emission was observed for a diode with compound substituted with anthracene units.

Thus, we conclude, that the most promising compound for further investigations is the imine with anthracene substituents.

Acknowledgements

Calculations have been carried out using resources provided by Wroclaw Centre for Networking and Supercomputing (http://wcss.pl), grant No. 18

Appendix A. Supplementary data

Supplementary data to this article can be found online at https://doi.org/10.1016/j.matchemphys.2019.122246.

References

[1] M. Koole, R. Frisenda, M.L. Petrus, M.L. Perrin, H.S.J. van der Zant, T. J. Dingemans, Charge transport through conjugated azomethine-based single molecules for optoelectronic applications, Org. Electron. 34 (2016) 38–41.
[2] W. Qin, S. Long, M. Panunzio, S. Biondi, Schiff bases: a short survey on an evergreen chemistry tool, Molecules 18 (2013) 12264–12289.
[3] V.K. Gupta, A.K. Singh, L.K. Kumawat, Thiazole Schiff base turn-on fluorescent chemosensor for Al^{3+} ion, Sens. Actuators B Chem. 195 (2014) 98–108.
[4] M.L. Petrus, R.K.M. Bouwer, U. Lafont, S. Athanasopoulos, N.C. Greenham, T. J. Dingemans, Small-molecule azomethines: organic photovoltaics via Schiff base condensation chemistry, J. Mater. Chem. 2 (2014) 9474–9477.
[5] W.A. Zoubi, Biological activities of schiff bases and their complexes: a review of recent works, Int. J. Org. Chem. 3 (2013) 73–95.
[6] L. Shi, W.J. Mao, Y. Yang, H.L. Zhu, Synthesis, characterization, and biological activity of a Schiff-base Zn(II) complex, J. Coord. Chem. 62 (2009) 3471–3477.

[7] A.W. Jeevadason, K.K. Murugavel, M.A. Neelakantan, Review on Schiff bases and their metal complexes as organic photovoltaic materials, Renew. Sustain. Energy Rev. 36 (2014) 220–227.
[8] S. Kotowicz, M. Siwy, S. Golba, J.G. Malecki, H. Janeczek, K. Smolarek, M. Szalkowski, D. Sek, M. Libera, S. Mackowski, E. Schab-Balcerzak, Spectroscopic, electrochemical, thermal properties and electroluminescence ability of new symmetric azomethines with thiophene core, J. Lumin. 192 (2017), 452–46.
[9] X. Zheng, W. Zhu, C. Zhang, Y. Zhang, C. Zhong, H. Li, G. Xie, X. Wang, C. Yang, Self-assembly of a highly emissive pure organic imine-based stack for electroluminescence and cell imaging, J. Am. Chem. Soc. 141 (2019) 4704–4710.
[10] A.N. Gusev, M.A. Kiskin, E.V. Braga, M. Chapran, G. Wiosna-Salyga, G. V. Baryshnikov, V.A. Minaeva, B.F. Minaev, K. Ivaniuk, P. Stakhira, H. Ågren, W. Linert, Novel zinc complex with an ethylenediamine schiff base for high-luminance blue fluorescent OLED applications, J. Phys. Chem. C 123 (2019), 11850−11859.
[11] S.K.J. Lim, R. Rahamathullah, N.M. Sarih, W.M. Khairul, Tailoring tail-free nematogen of ethynylated-schiff base and its evaluation as solution-processable OLED emitting material, J. Lumin. 201 (2018) 397–401.
[12] L. Yan, R. Li, W. Shen, Z. Qi, Multiple–color AIE coumarin–based Schiff bases and potential application in yellow OLEDs, J. Lumin. 194 (2018) 151–155.
[13] A. Iwan, D. Sek, Processible polyazomethines and polyketanils: from aerospace to light-emitting diodes and other advanced applications, Prog. Polym. Sci. 33 (2008) 289–345.
[14] B.C.E. Makhubela, M. Meyer, G.S. Smith, Evaluation of trimetallic Ru(II)- and Os (II)-Arene complexes as potential anticancer agents, J. Org. Chem. 772–773 (2014) 229–241.
[15] A.R. Burgoyne, C.H. Kaschula, M.I. Parker, G.S. Smith, Synthesis and anticancer evaluation of mono- and trinuclear half-sandwich rhodium(III) and iridium(III) complexes based on *N,O*-salicylaldiminato-sulfonated scaffolds, J. Org. Chem. 846 (2017) 100–104.
[16] A.R. Burgoyne, C.H. Kaschula, M.I. Parker, G.S. Smith, Tripodal half –sandwich rhodium and iridium complexes containig sulfonate and pyridinyl entities as antitumor agents, Eur. J. Inorg. Chem. 45 (2017) 5379–5386.
[17] A. Kilic, I. Koyuncu, M. Durgun, I. Ozaslan, I.H. Kaya, A. Gonel, Synthesis and characterization of the hemi-salen ligands and their triboron complexes: spectroscopy and examination of anticancer properties, Chem. Biodivers. 15 (2018) 1700428.
[18] M. Nath, P.K. Saini, A. Kumar, New di- and triorganotin(IV) complexes of tripodal Schiff base ligand containing three imidazole arms: synthesis, structural characterization, anti-inflammatory activity and thermal studies, J. Org. Chem. 695 (2010) 1353–1362.
[19] O. Alici, A novel tripodal colorimetric and fluorescence “turn on” chemosensor for AcO^- and F^- anions in CH_3CN, Spectrochim. Acta 167 (2016) 78–83.
[20] P. Kaur, J. Singh, R. Singh, V. Kaur, D. Talwar, Extending photophysical behavior of Schiff base tripod for the speciation of iron and fabrication of INHIBIT type molecular logic gate for fluorogenic recognition of Zn(II) and Cd(II) ions, Polyhedron 125 (2017) 230–237.
[21] A. Iwan, H. Janeczek, B. Kaczmarczyk, B. Jarząbek, M. Sobota, P. Romnon, Star-shaped azomethimes base on tris(2-aminoethyl)amine characterization, thermal and optical study, Spectrochim. Acta 75 (2010) 891–900.
[22] I. Ravikumar, B.N. Ahamed, P. Ghosh, Attachment of 4-methoxy benzyl units to a tripodal fluoroionophore shows reversal of output functionality with Cu(II) input, Tetrahedron 63 (2007) 12940–12947.
[23] M. Wenzel, K. Wichmann, K. Gloe, K. Gloe, K.J. Buschmann, K. Otho, M. Schroder, A.J. Blake, C. Wilson, A.M. Mills, L.F. Lindoy, P.G. Plieger, Interaction of tripodal Schiff-base ligands with silver(I): structural and solution studies, CrystEngComm 12 (2010) 4176–4183.
[24] M.J. Frisch, G.W. Trucks, H.B. Schlegel, G.E. Scuseria, M.A. Robb, J.R. Cheeseman, G. Scalmani, V. Barone, G.A. Petersson, H. Nakatsuji, LiX, M. Caricato, A. V. Marenich, J. Bloino, B.G. Janesko, R. Gomperts, B. Mennucci, H.P. Hratchian, J. V. Ortiz, A.F. Izmaylov, J.L. Sonnenberg, D. Williams-Young, F. Ding, F. Lipparini, F. Egidi, J. Goings, B. Peng, A. Petrone, T. Henderson, D. Ranasinghe, V. G. Zakrzewski, J. Gao, N. Rega, G. Zheng, W. Liang, M. Hada, M. Ehara, K. Toyota, R. Fukuda, J. Hasegawa, M. Ishida, T. Nakajima, Y. Honda, O. Kitao, H. Nakai, T. Vreven, K. Throssell, J.A. Montgomery Jr., J.E. Peralta, F. Ogliaro, M. J. Bearpark, J.J. Heyd, E.N. Brothers, K.N. Kudin, V.N. Staroverov, T.A. Keith, R. Kobayashi, J. Normand, K. Raghavachari, A.P. Rendell, J.C. Burant, S.S. Iyengar, J. Tomasi, M. Cossi, J.M. Millam, M. Klene, C. Adamo, R. Cammi, J.W. Ochterski, R.L. Martin, K. Morokuma, O. Farkas, J.B. Foresman, D.J. Fox, Gaussian 16, Revision B.01, Gaussian, Inc., Wallingford CT, 2016.
[25] P. Bujak, I. Kulszewicz-Bajer, M. Zagorska, V. Maurel, I. Wielgus, A. Pron, Polymers for electronics and spintronics, Chem. Soc. Rev. 42 (2013) 8895–8999.
[26] M. Lapkowski, P. Data, S. Golba, J. Soloducho, A. Nowakowska-Oleksy, Unusual band-gap migration of N-alkylcarbazole-thiophene derivative, Opt. Mater. 33 (2011) 1445–1448.
[27] D. Sęk, S. Kotowicz, S. Kula, M. Siwy, A. Szłapa-Kula, J.G. Małecki, S. Maćkowski, E. Schab-Balcerzak, Thermal, spectroscopic, electrochemical, and electroluminescent characterization of malononitrile derivatives with triphenylamine structure, Spectrochim. Acta 175 (2017) 168–176.
[28] D. Sęk, M. Siwy, K. Bijak, M. Filapek, G. Malecki, E.M. Nowak, J. Sanetra, A. Jarczyk-Jedryka, K. Laba, M. Lapkowski, E. Schab-Balcerzak, Optical and electrochemical properties of novel thermally stable Schiff bases bearing naphthalene unit, J. Electroanal. Chem. 751 (2015) 128–136.
[29] A. Bolduc, S. Dufresne, W.G. Skene, Chemical doping of EDOT azomethine derivatives: insight into the oxidative and hydrolytic stability, J. Mater. Chem. 22 (2012) 5053–5064.
[30] D.-Y. Lee, M.-H. Lee, C.-J. Lee, S.-K. Park, Driving characteristics of poly(N-vinylcarbazole) and 2-(4-biphenylyl)-5-(4-tert-butylphenyl)-1,3-4-oxadiazole-Based polymer light emitting diodes, Electron Mater Lett 9 (2013) 663–668.
[31] I. Glowacki, Z. Szamel, The nature of trapping sites and recombination centres in PVK and PVK–PBD electroluminescent matrices seen by spectrally resolved thermoluminescence, J. Phys. D Appl. Phys. 43 (2010) (2010) 295101.
[32] N.T. Kalyani, S.J. Dhoble, Organic light emitting diodes: energy saving lighting technology—a review, Renew. Sustain. Energy Rev. 16 (2012) 2696–2723.